Nanostructures

DOI: 10.1002/ange.201107681

Ultrathin $W_{18}O_{49}$ Nanowires with Diameters below 1 nm: Synthesis, Near-Infrared Absorption, Photoluminescence, and Photochemical Reduction of Carbon Dioxide**

Guangcheng Xi, Shuxin Ouyang, Peng Li, Jinhua Ye, Qiang Ma, Ning Su, Hua Bai, and Chao Wang*

Inorganic nanowires with ultrathin diameters below the magic size (i.e., less than 2 nm) and even one unit cell size, have attracted much research attention in the past few years owing to their unique chemical and physical properties.[1–9] As an important semiconductor material, tungsten oxide (WO_{3-x}) nanowires and nanorods have attracted considerable attention because of their wide applications in gas sensors, electrochromic windows, optical devices, and photocatalysts.[10–13] In particular, monoclinic $W_{18}O_{49}$ is of great interest owing to its unusual defect structure and promising properties in the nanometer regime.[14,15]

Early on, Park and co-workers reported the synthesis of $W_{18}O_{49}$ nanorods with a diameter of 4 nm by decomposing $[W(CO)_6]$ in $Me_3NO_2{\cdot}2H_2O$ and oleylamine.[16] Subsequently, Niederberger and co-workers synthesized hybrid $W_{18}O_{49}$/organic nanowires with a very thin diameter of 1.3 nm by a bioligand-assisted method.[17] Recently, Tremel and co-workers prepared $W_{18}O_{49}$ nanorods with a diameter of 2 nm by decomposing tungsten ethoxide in a mixture of oleic acid and trioctyl amine.[18] Although good control over nanocrystal dimensions can be realized in these methods, removal of the surfactants or organic residues from the nanowire surface requires multiple washing steps. For fundamental investigations on the ultrathin oxide nanowire itself, as well as for technological applications (such as sensing and catalysis), the presence of residues on the nanowire surface from the synthesis may be a significant drawback.

Herein, we report the preparation of ultrathin $W_{18}O_{49}$ nanowires that are efficient in the photochemical reduction of carbon dioxide by visible light. The ultrathin $W_{18}O_{49}$ nanowires were prepared by a very simple one-pot solution-phase method (see the experimental section in the Supporting Information). In a typical procedure, WCl_6 was dissolved in ethanol, and the clear yellow solution was transferred to a teflon-lined stainless-steel autoclave and heated at 180 °C for 24 h. A blue flocculent precipitate was collected, washed, dried in air, and obtained in a yield of approximately 100 %. The product is insoluble in water and in acid (HCl, pH 0), and has a high specific surface area.

$W_{18}O_{49}$ is a monoclinic structure type (P2 m) with lattice parameters of $a = 18.318$, $b = 3.782$, and $c = 14.028$ Å. Monoclinic $W_{18}O_{49}$ has a distorted ReO_3 structure in which corner-sharing distorted and tilt WO_6 octahedra are connected in the *a*-, *b*-, and *c*-direction, thereby forming a three-dimensional structure (inset in Figure 1 a). The X-ray diffraction (XRD) pattern of our sample demonstrates that the sample consists of monoclinic-phase $W_{18}O_{49}$ (Figure 1 a). The narrow (010) and (020) peaks strongly suggest that the possible crystal growth direction of the sample is [010], since the close-packed planes of the monoclinic $W_{18}O_{49}$ crystal are {010}, which will be further demonstrated by the direct observation of the high-resolution transmission electron microscopy (HRTEM) image (see below). Energy-dispersive X-ray spectroscopy (EDS) confirms that the sample only contains W and O elements (Figure 1 b). Furthermore, the Fourier transform infrared (FTIR) spectrum exhibits the clear surface of our sample (Figure S1 in the Supporting Information).

Scanning electron microscopy (SEM) and transmission electron microscopy (TEM) images show that the as-synthesized sample is composed of nanowires with large aspect ratio and lengths of up to several micrometers (Figure 1 c, d). Interestingly, higher-magnification TEM images (Figure 1 e and Figures S2 and S3 in the Supporting Information) clearly reveal that the nanowires shown in Figure 1 d are composed of a lot of individual, thinner nanowires. The diameter of the thinner nanowires is only about 0.9 nm. The HRTEM image and corresponding fast Fourier transform (FFT) pattern demonstrate that the ultrathin nanowires are crystalline and grow along [010] direction (Figure 1 f and Figure S4 in the Supporting Information). A comparison of the unit cell of $W_{18}O_{49}$ projected along the [010] direction with the typical diameter of the nanowires of 0.9 nm (red circle) allows

[*] Dr. G. C. Xi, Dr. S. X. Ouyang, P. Li, Prof. J. H. Ye
International Center for Materials Nanoarchitectonics (WPI-MANA), and
Environmental Remediation Materials Unit
National Institute for Materials Science (NIMS)
1-2-1 Sengen, Tsukuba, Ibaraki 305-0047 (Japan)
E-mail: jinhua.ye@nims.go.jp
Dr. G. C. Xi, Dr. Q. Ma, N. Su, Prof. H. Bai, Prof. C. Wang
Nanomaterials and Nanoproducts Research Center
Chinese Academy of Inspection and Quarantine
Beijing, 100123 (China)
Prof. J. H. Ye
TU-NIMS Joint Research Center
School of Material Science and Engineering, Tianjin University
92 Weijin Road, Tianjin (P.R. China)

[**] This work received financial support from the World Premier International Research Center Initiative (WPI Initiative) on Materials Nanoarchitectonics, the Natural Science Foundation of China (51102220), and the Global COE Program of Tokyo Institute of Technology (Japan).

Supporting information for this article is available on the WWW under http://dx.doi.org/10.1002/anie.201107681.

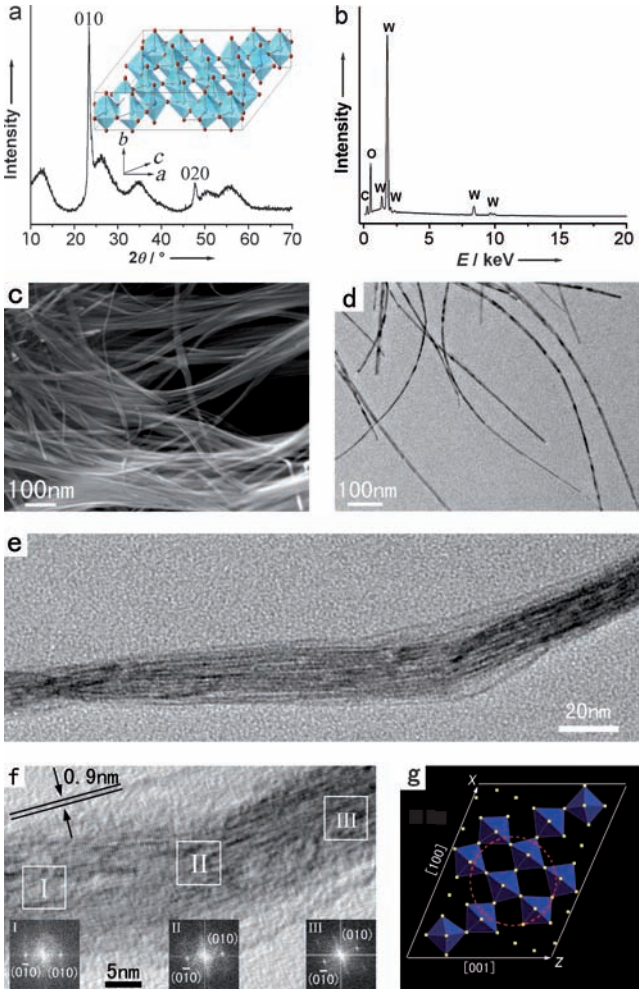

Figure 1. a) XRD pattern of the $W_{18}O_{49}$ nanowires, inset: crystal structure of monoclinic $W_{18}O_{49}$. b) EDS spectrum of the nanowires. c, d, e) SEM, TEM, and high-magnification TEM images, respectively, of the $W_{18}O_{49}$ nanowires. f) HRTEM image of the ultrathin nanowires. Insets: The corresponding FFT patterns of the areas I, II, and III. g) Schematic representation of the cross-section of a 0.9 nm nanowire inside one $W_{18}O_{49}$ unit cell oriented along the [010] direction.

{010}; thus, the nanocrystals of $W_{18}O_{49}$ would preferentially grow along the [010] direction. Since the diameter of the nanowires is very small (that is, their surface energy is very large), the nanowires tend to tangle with each other to reduce the surface energy. As a result, bundle-like nanowires were formed. Of course, the exact formation mechanism should be further investigated.

The $W_{18}O_{49}$ nanowires show unusual photophysical properties, as indicated by ultraviolet/visible (UV/Vis) absorption spectroscopy (Figure 2a). A very large absorption tail present

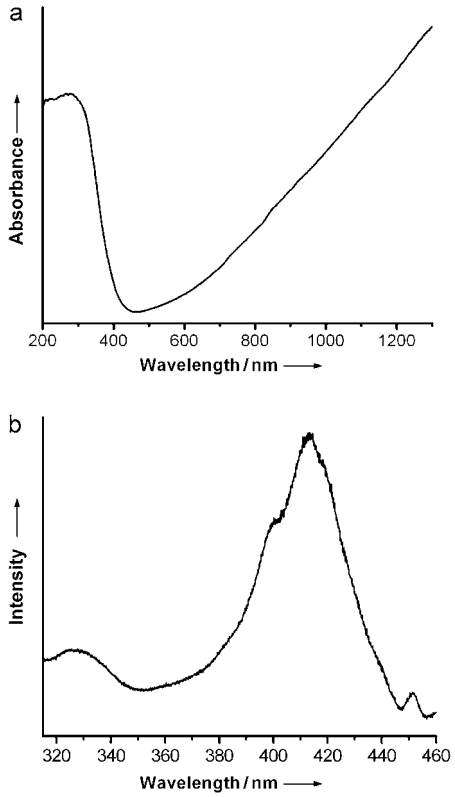

Figure 2. a) UV/Vis absorption spectrum and b) photoluminescence spectrum of the ultrathin $W_{18}O_{49}$ nanowires.

a rough estimation of the proportion of tungsten atoms present on the nanowire surface (Figure 1 g). The cross-section in the (010) plane contains about 8 tungsten atoms, and about 6 of them are located on the surface.

Experimental results showed that a low precursor concentration ($C_{WCl6} \leq 0.5$ g/100 mL) contributes to the formation of the ultrathin $W_{18}O_{49}$ nanowires. Once the precursor concentration was higher than 1.5 g/100 mL, sea-urchin-like nanostructures composed of a number of nanowires with larger diameters were obtained (Figure S5 in the Supporting Information). Polymer-assisted growth of bundle-like $BaSO_4$ and $BaCrO_4$ nanowires with larger diameters in solution has been reported.[19,20] Although the exact formation mechanism of the ultrathin $W_{18}O_{49}$ nanowire bundles is unknown at the moment, we believe the crystal-structure features of the $W_{18}O_{49}$ play an important role in the formation of the bundle-like nanowires. In this structure, the close-packed planes are in the visible and near infrared (NIR) regions of the absorption spectrum gives clear evidence that the nanowires consist of a large number of oxygen vacancies,[21] which is very different from those one-dimensional $W_{18}O_{49}$ nanostructures with larger diameters.[18,22] For those $W_{18}O_{49}$ nanowires with relatively larger diameters, no absorption was observed in the visible and NIR regions.

Photoluminescence (PL) spectra recorded at an excitation wavelength of 270 nm also demonstrated that the ultrathin nanowires contain a large number of oxygen vacancies (Figure 2b). The PL emission spectrum of the $W_{18}O_{49}$ nanowires recorded at room temperature shows an emission band at 3.78 eV (325 nm), which corresponds to the band-to-band transition. Compared with the reported band emission (3.60 eV) of $W_{18}O_{49}$ nanorods with a larger diameter (3 nm),[16] the large blue shift of the emission indicates that the as-synthesized ultrathin $W_{18}O_{49}$ nanowires possess

a strong quantum confinement effect. A blue emission band at 2.9 eV (420 nm), which may originate from the presence of oxygen vacancies or defects, was also found in the PL spectrum. In contrast to the previous report,[16,18] the intensity of this blue emission band is much higher than that of the band emission band, which further demonstrates that the prepared ultrathin nanowires contain a lot of oxygen vacancies.

Control experiments show that the color of a $W_{18}O_{49}$ sample gradually changed from blue in the original sample to yellow in the final sample (Figure 3a) once the sample was

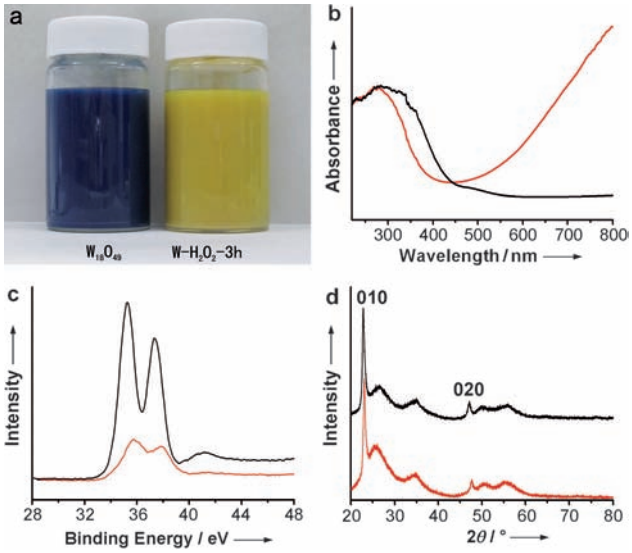

Figure 3. a) Color conversion, b) UV/Vis absorption spectra, c) XPS spectra, and d) XRD patterns of the ultrathin $W_{18}O_{49}$ nanowires before (red line) and after oxidation (black line) by H_2O_2.

oxidized with hydrogen peroxide (H_2O_2) for three hours. The corresponding absorption spectrum of the yellow sample (marked as W-H_2O_2-3 h) shows a clear red shift, and no absorption tail is present (black line, Figure 3b), which indicates that the oxygen vacancies in the surface of the nanowires disappear after oxidizing with H_2O_2. The change in the valence of W atoms in the nanowire surface before and after H_2O_2 treatment could be characterized by using X-ray photoelectron spectroscopy (XPS; Figure 3c). For the $W_{18}O_{49}$ nanowires, four peaks corresponding to W4f could be seen in the XPS spectrum. Two peaks observed at 35.71 and 37.81 eV correspond to W^{6+}, and the other two peaks at 34.78 and 37.07 eV correspond to W^{5+} (Figure 3c, red line).[23] For the W-H_2O_2-3 h sample (Figure 3c, black line), two sharp peaks of W4f and one weak peak of W5p can be seen in the spectrum, which is a typical feature of W^{6+}. The XPS spectra clearly demonstrated that after oxidizing with H_2O_2, the valence of W has changed to W^{6+}. This means that the oxygen vacancies in the surface of the nanowires disappear after oxidation with H_2O_2, which also explains the disappearing of the absorption tail in the absorption spectra.

We noted that although the color, UV/Vis absorption spectra, and XPS characterizations of the W-H_2O_2-3 h nanowires display distinct differences from the original $W_{18}O_{49}$ nanowires, the XRD patterns of W-H_2O_2-3 h and $W_{18}O_{49}$ are very similar (Figure 2d). This result clearly demonstrated that the oxidation only took place on the surface of the nanowires, and that the inside of the W-H_2O_2-3 h nanowires is still composed of $W_{18}O_{49}$.

Because crystal defects often give rise to unexpected results in chemical reactions, we investigated the photochemical activity of the oxygen-vacancy-rich $W_{18}O_{49}$ nanowires by the photochemical reduction of $CO_2 + H_2O$ vapor in a gas-solid system. The $W_{18}O_{49}$ nanowires achieved efficient methane production from carbon dioxide and water vapor on illumination with visible light ($\lambda > 420$ nm) in the absence of noble-metal co-catalysts such as Pt and Au (Figure 4a). The average formation rate of methane is about 666 ppm $g^{-1} h^{-1}$

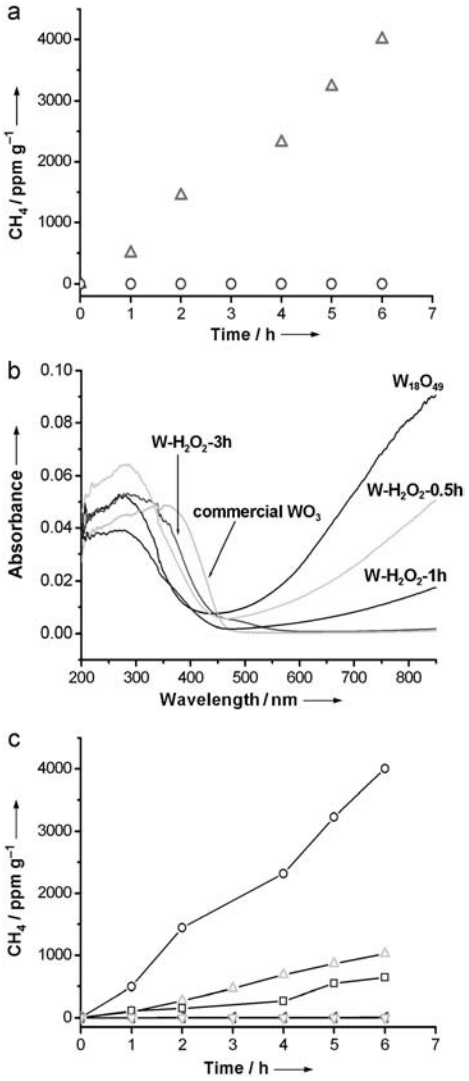

Figure 4. a) Time courses of CH_4 production over the as-synthesized $W_{18}O_{49}$ nanowires under visible light ($\lambda \geq 420$ nm, △) and in the dark at 70 °C (○). b) UV/Vis absorption spectra of the tungsten oxide samples obtained by oxidation with H_2O_2 for different time periods. c) Time courses of CH_4 production over the tungsten oxide samples with different oxygen-vacancy concentrations. $W_{18}O_{49}$ (○), W-H_2O_2-0.5 h (△), W-H_2O_2-1 h (□), and W-H_2O_2-3 h and commercial WO_3 overlapping (▽, ◁).

(0.029 mmol $L^{-1} g^{-1} h^{-1}$). Besides methane, only 5% (molar ratio) of other hydrocarbons (such as ethanol and acetone) were produced, which suggests that the selectivity of this photochemical reaction is very high. Because the equilibrium temperature of the photochemical reaction system was about 70 °C (± 4 °C), control experiments were carried out to detect the influence of temperature on product formation. The experiments showed that no methane was detected when the reactions were performed in the dark at 70 °C, that is, the reduction of carbon dioxide cannot be started in the absence of light. Therefore, the formation of methane is really based on a photopromoted reduction of carbon dioxide. To our knowledge, the photochemical conversion of carbon dioxide into methane over $W_{18}O_{49}$ under visible light has not been reported to date. Furthermore, the formation rate of methane increased rapidly, up to 50000 ppm $g^{-1} h^{-1}$ (2.2 mmol $L^{-1} g^{-1} h^{-1}$), when a full-arc xenon lamp was used as the light source.

We then investigated the effect of the concentration of oxygen vacancies on the photochemical reduction of carbon dioxide. By adjusting the H_2O_2 treating time, a series of tungsten oxide samples with different oxygen-vacancy concentrations was prepared. UV/Vis absorption spectra show the oxygen-vacancy concentrations of the samples gradually reduced as the oxidation time increased (Figure 4b). Figure 4c shows the rate of methane evolution on tungsten oxide catalysts with different concentrations of oxygen vacancies. After oxidizing for 0.5 h, the activity of methane evolution on the sample is reduced down to 25% (170 ppm $g^{-1} h^{-1}$). After oxidizing for 1 h, the sample shows activity in photochemical methane evolution, but the rate of methane evolution is lower (106 ppm $g^{-1} h^{-1}$). No methane or other kinds of hydrocarbons were detected when W-H_2O_2-3 h was used as the catalyst, the surface of which was completely oxidized into W^{6+} by H_2O_2, thus suggesting that WO_3 is not active for photocatalytic methane evolution, which is in agreement with previous studies. We also investigated the properties of the samples after 30 h photochemical reaction, and found that the oxygen-vacancy concentration in the samples was greatly reduced (Figure S6 in the Supporting Information). However, the size and morphology of the nanowires were not affected by this reaction process (Figure S7 in the Supporting Information). These experimental results demonstrated unambiguously that oxygen vacancies in the samples play a very important role in the photocatalytic methane evolution under visible light.

Our experimental results showed that once all of the oxygen vacancies in the ultrathin nanowires were consumed by carbon dioxide molecules, no methane molecules were generated. Generally, the oxygen vacancies would be fully consumed after irradiation with visible light ($\lambda \geq 420$ nm, 30 mW cm^{-2}) for 90 h in the presence of carbon dioxide (1 atm) and water (0.8 mL), and the color of the nanowires changed from blue to yellow-green. Fortunately, by utilizing the strong reducing power of $NaBH_4$, we found that the activity of the nanowires could be easily recovered (for details see the experimental section in the Supporting Information). Control experiments showed that the size and morphology of the nanowires were not affected by this treatment (Figures S8–S10 in the Supporting Information).

Although the exact mechanism for the photochemical formation of methane over the ultrathin $W_{18}O_{49}$ nanowires is not clear, we believe that the oxygen vacancies contained in the nanowires provide a large quantity of reductive sites in the conversion from carbon dioxide into methane. By consuming oxygen vacancies, one carbon dioxide molecule is reduced to one methane molecule. Furthermore, since a large number of oxygen vacancies exists in the nanowires, with a "trap" effect (Figure S11 in the Supporting Information), they can tightly "catch" carbon dioxide molecules and greatly enhance the adsorption of carbon dioxide.[24] The attraction between an oxygen vacancy and a carbon dioxide molecule may generate an unexpected affinity interaction and therefore lower the reactive barrier. Moreover, the oxygen vacancies can absorb visible light effectively and provide more active sites for reaction. More details of the mechanism are being studied.

In summary, ultrathin $W_{18}O_{49}$ nanowires were synthesized by a simple one-pot solution method. The nanowires are only about 0.9 nm in diameter and contain a large number of oxygen vacancies. The ultrathin nanowires show strong light absorption from the visible to the NIR region. The oxygen-vacancy-rich ultrathin $W_{18}O_{49}$ nanowires show an excellent capability of photochemical reduction of carbon dioxide under irradiation with visible light. This work presents not only a possibility for the use of ultrathin $W_{18}O_{49}$ nanowires as a functional material in the conversion of carbon dioxide but also an important concept that oxygen-vacancy-rich non-stoichiometric simple oxides can be used as a new strategy to design materials with high photochemical activity.

Received: November 1, 2011
Published online: January 26, 2012

Keywords: carbon dioxide · nanowires · oxygen vacancies · photochemistry · tungsten

[1] C. Wang, Y. Hu, C. M. Lieber, S. Sun, *J. Am. Chem. Soc.* **2008**, *130*, 8902.
[2] Z. Huo, C. K. Tsung, W. Huang, M. Fardy, R. Yan, X. Zhang, Y. Li, P. Yang, *Nano Lett.* **2009**, *9*, 1260.
[3] L. Cademartiri, G. A. Ozin, *Adv. Mater.* **2009**, *21*, 1013.
[4] X. Lu, M. S. Yavuz, H. Y. Tuan, B. A. Korgel, Y. Xia, *J. Am. Chem. Soc.* **2008**, *130*, 8900.
[5] J. W. Liu, J. H. Zhu, C. L. Zhang, H. W. Liang, S. H. Yu, *J. Am. Chem. Soc.* **2010**, *132*, 8945.
[6] X. X. Xu, J. Zhuang, X. Wang, *J. Am. Chem. Soc.* **2008**, *130*, 12527.
[7] X. Hong, D. S. Wang, R. Yu, H. Yan, Y. Sun, L. He, Z. Niu, Q. Peng, Y. D. Li, *Chem. Commun.* **2011**, *47*, 5160.
[8] Y. P. Du, Y. W. Zhang, Z. G. Yan, L. D. Sun, C. H. Yan, *J. Am. Chem. Soc.* **2009**, *131*, 16364.
[9] X. W. Teng, W. Q. Han, W. Ku, M. Hucker, *Angew. Chem.* **2008**, *120*, 2085; *Angew. Chem. Int. Ed.* **2008**, *47*, 2055.
[10] D. Chen, J. H. Ye, *Adv. Funct. Mater.* **2008**, *18*, 1922.
[11] G. C. Xi, B. Yue, J. Y. Cao, J. H. Ye, *Chem. Eur. J.* **2011**, *17*, 5145.
[12] R. Abe, H. Takami, N. Murakami, B. Ohtani, *J. Am. Chem. Soc.* **2008**, *130*, 7780.
[13] D. L. Chen, L. Gao, A. Yasumori, K. Kroda, Y. Sugahara, *Small* **2008**, *4*, 1813.
[14] G. Gu, B. Zheng, W. Q. Han, S. Roth, J. Liu, *Nano. Lett.* **2002**, *2*, 849.

[15] X. W. Lou, H. C. Zeng, *Inorg. Chem.* **2003**, *42*, 6169.
[16] K. Lee, W. S. Seo, J. T. Park, *J. Am. Chem. Soc.* **2003**, *125*, 3408.
[17] J. Polleux, N. Pinna, M. Antonietti, M. Niederberger, *J. Am. Chem. Soc.* **2005**, *127*, 15595.
[18] A. Yella, M. N. Tahir, S. Meuer, R. Zentel, R. Berger, M. Panthofer, W. Tremel, *J. Am. Chem. Soc.* **2009**, *131*, 17566.
[19] S. H. Yu, M. Antonietti, H. Colfen, J. Hartmann, *Nano Lett.* **2003**, *3*, 379.
[20] S. H. Yu, H. Colfen, M. Antonietti, *Chem. Eur. J.* **2002**, *8*, 2937.
[21] T. Nütz, M. Haase, *J. Phys. Chem. B* **2000**, *104*, 8430.
[22] C. Y. Su, H. C. Lin, *J. Phys. Chem. C* **2009**, *113*, 4042.
[23] M. Feng, A. Pan, H. Zhang, Z. Li, F. Liu, H. Liu, D. Shi, B. Zou, H. Gao, *Appl. Phys. Lett.* **2005**, *86*, 141901.
[24] K. Xie, N. Umezawa, N. Zhang, P. Reunchan, Y. J. Zhang, J. H. Ye, *Energy Environ. Sci.* **2011**, *4*, 4211.

